HHS Public Access

Author manuscript

Exp Eye Res. Author manuscript; available in PMC 2020 February 01.

Published in final edited form as:

Exp Eye Res. 2019 February ; 179: 106–114. doi:10.1016/j.exer.2018.11.010.

Photoreceptor degeneration in a new *Cacna1f* mutant mouse model

Xufeng Dai[#a,b], **Shiyi Pang**[#c,d], **Jieping Wang**[c], **Bernard FitzMaurice**[c], **Jijing Pang**[a,b,d,e,**], and **Bo Chang**[c,*]

[a]School of Ophthalmology and Optometry, The Eye Hospital, Wenzhou Medical University, Wenzhou, Zhejiang 325027, China

[b]Department of Ophthalmology, University of Florida, Gainesville, FL 32610, USA

[c]The Jackson Laboratory, Bar Harbor, ME 04609, USA

[d]College of Medicine, University of Florida, Gainesville, FL 32610, USA

[e]Eye Research Institute, Xiamen Eye Center of Xiamen University, Xiamen 361001, China

[#] These authors contributed equally to this work.

Abstract

The *Cacna1f* gene encodes the α1F subunit of an L-type voltage-gated calcium channel, Cav1.4. In photoreceptor synaptic terminals, Cav1.4 channels mediate glutamate release and postsynaptic responses associated with visual signal transmission. We have discovered a new *Cacna1f* mutation in *nob9* mice, which display more severe phenotypes than do *nob2* mice. To characterize the *nob9* phenotype at different ages, we examined the murine fundus, applied retinal optical coherence tomography, measured flash electroretinograms (ERGs) in vivo, and analyzed the retinal histology in vitro. After identifying the X-linked recessive inheritance trait, we sequenced *Cacna1f* as the candidate gene. Mutations in this gene were detected by polymerase chain reaction (PCR) and confirmed by restriction fragment length polymorphism. Morphologically, an early-onset of retinal disorder was detected, and the degeneration of the outer plexiform layers progressed rapidly. Moreover, the mutant mice showed drastically reduced scotopic ERGs with increasing age. In 14-month-old *nob9* retinas, immunostaining of cone opsins demonstrated a reduction in the number of short-wavelength opsins (S-opsins) to 54% of wild-type levels, and almost no middle-wavelength opsins (M-opsins) were observed. No cone ERGs could be detected from residual cones, in which S-opsins abnormally migrated to inner segments of the photoreceptors. The

[*]Corresponding author. bo.chang@jax.org (B. Chang). [**]Corresponding author. jpangoph@hotmail.com (J. Pang).

Author contributions

Xufeng Dai and Shiyi Pang contributed equally in performing most of the experiments, taking part in the work involved in image processing and writing of the manuscript; Bo Chang designed the study project and was responsible for supervisory control; Jieping Wang helped with several experiments; Bernard FitzMaurice offered materials and technical support for the study; Jijing Pang contributed to the revision of the manuscript. All authors have read and approved the final article.

Conflicts of interest

The authors have no financial or nonfinancial conflicts of interests to declare.

mutations of the *Cacna1f* gene in *nob9* mice involved both a single nucleotide G to A transition and a 10-nucleotide insertion, the latter resulting in a frame-shift mutation in exon 14.

Keywords

Congenital stationary night blindness; X-linked recessive inheritance; Mice; Electroretinogram; Cone opsins

1. Introduction

The *Cacna1f* gene encodes the α1F subunit of an L-type voltage-gated calcium channel, Cav1.4 (Bech-Hansen et al., 1998; Boycott et al., 2001; Fisher et al., 1997). In the retina, Cav1.4 channels are localized to the synaptic layers, including the outer and inner plexiform layers (OPLs and IPLs); more specifically, they are localized to the ribbon synapses of photoreceptors and bipolar cells (Morgans, 2001; Regus-Leidig et al., 2014). Immunohistochemistry with α1F-specific antibodies confirmed localization of these channels at the plasma membrane in the base of the ribbon (Morgans et al., 2005). In photoreceptor synaptic terminals, Cav1.4 channels mediate glutamate release and postsynaptic responses associated with visual signal transmission (Liu et al., 2013). Defects in retinal Cav1.4 subunits reduce the synaptic transfer efficacy from photoreceptors to second-order retinal neurons (i.e., bipolar and horizontal cells).

The *nob2 (no b-wave 2)* mouse is an animal model with a naturally occurring *Cacna1f* mutation (Chang et al., 2006). The *Cacna1f* gene in this mouse is disrupted by a transposable element insertion in exon 2, resulting in a truncated protein product (Bayley and Morgans, 2007; Chang et al., 2006). Consequently, electroretinogram (ERG) b-wave responses in this mouse are reduced, but not absent. This is consistent with data from a *Cacna1f* knockout mouse model, which shows a dramatic reduction in depolarization-induced calcium influx into photoreceptor terminals (Mansergh et al., 2005). In addition, some *Cacna1f*-deficient mice have horizontal and rod bipolar cells that extend ectopic neurites into the retinal outer nuclear layer (ONL) and beyond, which leads to a collapse of the OPL (Bayley and Morgans, 2007; Chang et al., 2006; Doering et al., 2008; Lodha et al., 2010; Mansergh et al., 2005). The characterization of *nob2* mice also revealed an abnormal bipolar and horizontal cell morphology and even altered retinal ganglion cell responses (Chang et al., 2006). Furthermore, *Cacna1f* knockout mice display photoreceptor degeneration (Knoflach et al., 2013; Knoflach et al., 2015; Mansergh et al., 2005; Michalakis et al., 2014; Regus-Leidig et al., 2014). A study in zebrafish confirmed that *Cacna1f* is also vital for the functional assembly and maintenance of cone photoreceptors (Jia et al., 2014).

The *nob2* mouse has stable dark-adapted ERG abnormalities but maintains partial cone responses (Chang et al., 2006). Here, we report a new naturally occurring animal model of *Cacna1f* mutation, the *nob9* mouse, which displays more severe phenotypes than *nob2* mice. After the novel mutations within the *Cacna1f* gene were identified by us, *nob9* retinas were analyzed using histology and ERGs to evaluate structural and functional characteristics. With cone-specific peanut agglutinin (PNA) and two types of cone opsin markers, we also

explored whether middle-wavelength opsins (M-opsins) and/or short-wavelength opsins (S-opsins) within cone photoreceptors display abnormalities.

2. Material and methods

2.1. Animals

All animals were maintained in the animal facilities of the University of Florida (Gainesville, FL) and The Jackson Laboratory (Bar Harbor, ME) on a 12/12-h light-dark cycle with an ambient light intensity of 15 lux. Mice were maintained under standard laboratory conditions (18–23°C, 40–65% humidity) with free access to food and water. Experimental results were obtained from mice between 2 days and 14 months of age.

All animal experiments complied with the Animal Research: Reporting of In Vivo Experiments (ARRIVE) guidelines and were conducted in accordance with the U.K. Animals (Scientific Procedures) Act, 1986 and associated guidelines, the EU Directive 2010/63/EU for animal experiments, and the National Institutes of Health (NIH) Guide for the Care and Use of Laboratory Animals (NIH Publications No. 8023, revised 1978). All experiments were approved by both the University of Florida and the Jackson Laboratory Institutional Animal Care and Use Committees (IACUCs).

2.2. Establishment of the *nob9* mouse strain

The *nob9* was discovered in a male mouse from the inbred mouse strain C57BL/6J-Chr $10.3^{PWD/PH}$/ForeJ (Stock No: 006599). This male mouse had significantly reduced rod ERG b-waves and was mated to C57BL/6J female mice with normal ERGs. The F1 progeny, which had normal ERGs, were intercrossed. In this F2 offspring, we identified only 4 male mice with reduced b-waves in the ERG, while 12 females and 3 males were unremarkable. This result indicated that the reduced b-wave might be inherited as an X-linked recessive pattern. Subsequently, the *nob9* was maintained by repeated backcrossing to C57BL/6J for five generations to make a congenic inbred strain, *B6.PWD-Cacna1f*^{nob9}/Boc (Stock No. 008805).

2.3. Gene mapping and sequencing

Total RNA was isolated from retinas of newborn mice with TRIZOL LS Reagent (Invitrogen Life Technologies, Carlsbad, CA), and the SuperScript preamplification system (Invitrogen Life Technologies) was used to synthesize first-strand cDNA. Due to phenotypic similarity to the *nob2* mice (Chang et al., 2006), *Cacna1f* was tried as the candidate gene to explore any mutations in the *nob9.* Eight pairs of overlapping PCR primers were used to amplify the entire open reading frame of the gene from cDNA (Table 1).

For PCR amplification, 25 ng DNA was used in a 10 μL volume containing 50 mM KCl, 10 mM Tris-HCl, 2.5 mM $MgCl_2$, 0.2 mM oligonucleotides, 200 mM dNTPs, and 0.02 U AmpliTaq DNA polymerase (pH = 8.3). Unless specified otherwise, all drugs were purchased from Sigma-Aldrich (St. Louis, MO, USA). The reactions were initially denatured for 3 min at 94°C and then subjected to 40 cycles of 15 s at 94°C, 1 min at 51°C, 1 min at 72°C, and a final 7-min extension at 72°C. PCR products were separated by

electrophoresis on 2% SeaKem LE (Cambrex, Rockland, ME) agarose gels, stained with ethidium bromide, and visualized under UV light. DNA was purified from cut gel bands using the QIAquick Gel Extraction Kit (Qiagen) and sequenced directly using standard fluorescent-based sequencing methods. To sequence the candidate intron 13–14, DNA was isolated from tail snips according to previously reported methods (Buffone and Darlington, 1985). PCR and sequencing were performed as described above, using a pair of primers specific to the targeted region: forward (CA-g13): 5-CTCACAAAGGGTGACTCTGG, reverse (CA-e14): 5'-GCAGAGCAGAACTTTGTTGG.

2.4. Restriction enzyme genotyping

To confirm the single nucleotide transition, a restriction endonuclease *BsaJI* (New England Biolabs, MA) was used to recognize and cleave DNA at "CCNNGG" sites (Wang et al., 2015). From PCR products, 5 ng of DNA was placed in 2.5 μL of 1X NEBuffer 2 and digested in 16.5 μL of *BsaJI* enzyme for 12 h at 60°C. Following digestion, the wild-type (WT) and *nob9* PCR products were separated on 2% SeaKem LE (Cambrex, Rockland, ME) agarose gel, stained with ethidium bromide, and visualized under UV light. Undigested PCR products of WT and *nob9* DNA were used for controls.

2.5. Fundus and retinal optical coherence tomography (OCT) evaluation

Eyes of all mice used in the characterization studies were dilated with 1% atropine ophthalmic drops (Bausch and Lomb Pharmaceuticals Inc., Tampa, FL) and were evaluated in vivo by a Micron III, a brightfield retinal imaging microscope equipped with image-guided OCT capabilities (Phoenix Laboratories, Inc). Animals were anesthetized by intraperitoneal injection with a solution of ketamine (70 mg/kg) and xylazine (5 mg/kg). The fundus and retinal OCT imaging system has a platform designed for mice that can freely orient and align the subject. Drops of 2.5% hydroxypropyl methylcellulose were applied to eyes to prevent corneal dehydration. The fundus photograph was always centered on the optic nerve (ON). Through the center of the ON, a retinal OCT image (nasal to temporal) was acquired.

2.6. ERG recordings

Mice were dark-adapted overnight (≥12 h) and anesthetized under dim red light. Pupils were thoroughly dilated with 1% tropicamide. To prevent corneal dehydration and allow for better electrical contact, 1% methylcellulose gel was applied to the recorded eyes. Mice were placed on a heating platform throughout the recording session to maintain body temperature. ERGs were recorded using a small contact lens electrode (Hansen Ophthalmics, Iowa City, IA), which was placed on the surface of the cornea. A needle-shaped reference electrode was placed under the skin of forehead, and a ground electrode was inserted subcutaneously near the tail. ERG responses were detected using a custom-built Ganzfeld dome and a computer-based system (Roland Consult, Wiesbaden, Germany or LKC Technologies, Gaithersburg, MD). Scotopic ERGs were recorded in responses to 0.03 and 3 cd-s/m^2 strengths white-light stimuli. The temporal frequency of flash presentation was set at 0.03 Hz under dark adaptation. Five responses were recorded and averaged. After a 10-min period of rod-desensitizing light adaptation (30 cd/m^2 brightness), photopic ERG was detected in response to a 30 cd-s/m^2 strength white-light stimulus. In addition, green (511 nm) and ultraviolet

(UV, 363 nm) light-emitting diodes were used as the stimulation light source for detecting M- and S-cone sensitive ERGs of mice, respectively (Dai et al., 2016). As optimal strengths, green light was set at 0.75 cd-s/m^2 and UV at 3 mW-s/m^2 (Dai et al., 2016). The temporal frequency of flash presentation was set at 1.0 Hz under light adaptation. To increase the signal:noise ratio, fifty responses were averaged. The duration of one stimulus was 2 ms, and the band pass of the amplifiers was set at 0.2–500 Hz. Amplitude of negative a-wave was measured from the pre-stimulus baseline to the trough of ERG waveform, while the amplitude of b-wave was measured from the trough to the following peak at a relatively fixed time (scotopic b-wave: approximately 70 ms, photopic b-wave: approximately 50 ms).

2.7. Structural analysis of the retina

Mice were sacrificed by inhalation of carbon dioxide. Eyes were enucleated and prepared for light microscopic examination. Briefly, eyes were fixed in Bouin's fixative at room temperature. Eyecups were rinsed in phosphate-buffered saline, dehydrated, and embedded in paraffin. On an RM 2135 microtome (Leica Microsystems, Wetzlar, Germany), 4 μm-thick sections were cut. Sections were mounted onto slides, rehydrated, and stained with hematoxylin and eosin. Slides were viewed under a light microscope (Olympus BX40, Japan) and pictures were taken with an attached camera (Olympus DP70, Japan).

2.8. Immunohistochemistry

Enucleated eyes were fixed overnight in 4% paraformaldehyde (4°C) after removing the cornea from each eye. Retinal whole mounts or sections were prepared as described previously (Li et al., 2011). Sequentially, retinal whole mounts and cryosections were permeated with 0.1% Triton X-100, rinsed in 0.1 M PBS, and blocked in 5% bovine serum albumin (BSA). FITC-conjugated PNA (1:400; Vector Laboratories, Burlingame, CA) was used to identify the interphotoreceptor matrix sheath that surrounds the cone outer segments. The specimens were incubated in M-or S-opsin primary antibodies (1:400; Santa Cruz Biotechnology, Santa Cruz, CA) overnight at 4°C. The retinas were washed 3 times with PBS and incubated with IgG secondary antibody tagged with Alexa-594 (molecular Probes, Eugene, OR) diluted 1:500 in PBS at room temperature for 1 hour. The nuclei were stained with 4', 6-diamidino-2- phenylindole. Retinal whole mounts and sections were mounted with coverslips for imaging by fluorescence microscopy. In retinal whole mounts, M-or S-opsins were manually counted 0.3 mm ventral to the optic nerve (Dai et al., 2016) within one field (53,652 μm^2) at high magnification (*40).

2.9. Statistical analysis

Six mice per group were analyzed. Statistical analysis was performed with SPSS (v18.0, IBM Corporation, Armonk, NY). Independent samples t-tests were used for data comparison between *nob9* and WT mice. Data are presented as mean ± standard deviation (SD). $P < 0.05$ was considered statistically significant.

3. Results

3.1. Retinal phenotypes in *nob9* mice

Compared with WT mice, the genetic mutation in *nob9* mice modified their retinal phenotype (Fig. 1). To identify early functional alterations, we selected 1-month-old mice to perform scotopic ERGs. The b-wave size was greatly reduced in *nob9* mice (Figs. 1A-B), but not absent. In addition, eyes from *nob9* mice also displayed small oscillatory potentials upon the flat b-wave (Fig. 1A). Morphologically, both *nob9* (Fig. 1C) and *nob2* mice (Chang et al., 2006) displayed a similarly thin retinal OPL, consistent with synaptic disorganization in the photoreceptor synaptic layer. In the *nob9* retina, the OPL showed a substantial reduction in thickness, whereas other layers did not (Fig. 1D).

3.2. Identification of sequence variants in the *nob9 Cacna1f* gene

We targeted the X-linked *Cacna1f* gene as the first candidate to test mutations. Mutations of the *nob2* mouse occurred in exon 2 of *Cacna1f* (Chang et al., 2006). But the *nob9* strain revealed different variations of the same gene; the novel mutations occurred between exon 13 and 14. One of the alterations was detected in a single nucleotide G to A transition near the end of intron 13–14 (Fig. 2A), and this mutation was further confirmed by PCR products digested by the restriction endonuclease *BsaJI.* Undigested PCR products of WT and *nob9* DNA were used as controls, which exhibited single DNA band, as did the digested *nob9* sample (Fig. 2B). In contrast, the digested C57BL/6J DNA displayed two bands of expected sizes (Fig. 2B), confirming the G mutation as shown in Fig. 2A. The second sequence alteration was a 10-nucleotide insertion between exon 13 and 14 of the *Cacna1f* gene. The insertion was near the G to A transition and located at the 3*'* end region within intron 13–14 (Fig. 2A). All *nob9* mice exhibit both variants.

3.3. Postnatal retinal development and OPL degeneration in *nob9* mice

The course of OPL maturation and degeneration was characterized at the histological level in *nob9* mice between postnatal day 2 (P2) and 14 months. Fig. 3 shows postnatal developments of their retina with gradual division and maturation between the ONL and the inner nuclear layer (INL). At P2, both the *nob9* and WT eyes exhibited similar structures across all retinal sections, which consisted only of an outer neuroblastic layer (NL) and an inner ganglion cell layer. Within the NL, an OPL gradually started to separate an ONL and INL around P6. The OPL in the WT retina exhibited nearly normal thickness at P10 when the *nob9* also showed the most visible space between ONL and INL (Fig. 3). The thickness of the *nob9* OPL increased from P6 until P10 and decreased at the time of eyelids opening (P14). This decrease was consistent with the degeneration of the synaptic layers between ONL and INL (Chang et al., 2006). We additionally examined fundus and retinal OCT in vivo. After 2 and up to 14 months, the space between ONL and INL was almost absent in *nob9* retinas (Figs. 3–4). The mutant mouse showed a normal fundus at 2 and 4 months, but some additional small discrete white dots were noted by the age of 8 months, mainly in the central and ventral quadrants (Fig. 4).

3.4. Age-dependent reduction of scotopic ERGs in *nob9* mice

To test retinal function over an extended period, we performed ERG recordings in 2-to 14-month old *nob9* mice. The *nob2* mice were reported to display stable ERG responses at 3–15 months (Chang et al., 2006). In *nob9* mice, scotopic ERG responses declined with increasing age (Fig. 5A). The average a-wave amplitude of a 2-month-old *nob9* mouse was about half of that from an age-matched WT mouse (independent samples t-test, $P < 0.001$; Fig. 5C). The size of the negative a-wave decreased continually up to 14 months, the last time point examined. At 14 months, the average *nob9* a-wave amplitude was reduced to 27% of the WT level (independent samples t-test, $P < 0.001$; Fig. 5C). Compared with the *nob2* mouse (Chang et al., 2006), photopic ERGs were more drastically affected in *nob9* animals, displaying nearly no waveform after 2 months (Figs. 5B and D).

3.5. Age-dependent reduction of cone opsins in *nob9* retinas

As mentioned above, photopic ERG responses in *nob9* mice were more severely affected. Therefore, we examined the presence of cone opsins in *nob9* retinas between the age of 2 and 14 months using cone-specific PNA and two types of cone opsin markers. Fig. 6A shows retinal whole mounts. Compared with age-matched WT retinas, the *nob9* had similar counts for the two opsins at 2 months (independent samples t-test, $P = 0.388$ for M-opsins, $P = 0.064$ for S-opsins), but with increasing age, these counts declined, especially for M-opsins (Figs. 6B-C). At 14 months, S-opsin counts of *nob9* retinas were diminished to 54% of the WT counts (independent samples t-test, $P < 0.001$; Fig. 6C) with almost no M-opsins detectable ($P < 0.001$, Fig. 6B).

Cross sections of 14-month-old *nob9* retinas not only confirmed the nearly total loss of M-opsins but also presented some PNA and S-opsins abnormally migrated to inner photoreceptors segments (Fig. 7).

3.6. Neither M- nor S-cone ERG responses detected in *nob9* eyes

There are only two classes of cones in mouse retinas, having peak wavelength sensitivities of about 511 nm (M-cones) and 359 nm (S-cones) (Jacobs and Williams, 2007; Li et al., 2011). Therefore, we used green ($\lambda = 511$ nm) and UV light ($\lambda = 363$ nm) stimuli to distinguish subtype activities. In this study, neither white (Fig. 5B) nor green light stimuli (Fig. 8) could elicit any M-cone ERG responses from *nob9* eyes.

Further, we used UV light to excite murine S-cones (Dai et al., 2016). As an optimal strength for normal WT eyes, the UV stimulus was set at 3 mW-s/m^2. However, no UV ERG responses from *nob9* cones could be detected (Fig. 8).

4. Discussion

In this study, we report a new animal model, the *nob9* mouse presenting spontaneous *Cacna1f* mutations, involving both a single nucleotide transition and a 10-nucleotide insertion between exon 13 and 14. The insertion causes a frame-shift mutation in exon 14. These mutations are completely different from that of the *nob2 Cacna1f,* the latter is disrupted by a transposable element insertion in exon 2 (Chang et al., 2006). In addition to

the *nob2* and *9* with naturally occurring *Cacna1f* mutation, several other murine models have been generated to characterize the effects of various *Cacna1f* mutations on retinal development, morphology and function (Mansergh et al., 2005; Regus-Leidig et al., 2014; Waldner et al., 2018).

Photoreceptor Cav1.4 is required for calcium influx and synaptic vesicle fusion (Matthews and Fuchs, 2010). In mouse retina, *Cacna1f* is expressed in multiple layers, involving OPL and IPL (Mansergh et al., 2005). The expression is consistent with the distribution pattern of synaptic ribbons in photoreceptors and bipolar cells (Sterling and Matthews, 2005). Encoded by *Cacna1f* gene, the Cav1.4 α1F subunit in the outer retina has been implicated in the structural and functional maintenance of photoreceptor synapses, which mediate release of neurotransmitters from photoreceptor terminals in response to light stimulation (Bech-Hansen et al., 1998; Boycott et al., 2001; Fisher et al., 1997). In the outer retina, the α1F subunit is expressed in OPL and localized to both rod and cone photoreceptor terminals (Chang et al., 2006; Morgans et al., 2005). Defects in the Cav1.4 α1F subunit impair synaptic transmission, and ERG b-wave reduction suggests the key role of the subunit in the control of glutamate release from photoreceptor (Catterall et al., 2008).

ERG examinations were performed in 1-month-old *nob9* animals to identify early functional alterations. Reflecting the activity of depolarizing bipolar cells (Pardue and Peachey, 2014), ERG b-waves of the mutant mice were significantly reduced under dark-adapted conditions but, as observed in other related animal models (Chang et al., 2006), were not absent. Corresponding to the defective signal transmission between photoreceptors and bipolar cells, the morphological analysis revealed a significantly attenuated OPL. The postnatal development of this photoreceptor synaptic layer was characterized in mice at the histological level. The thickness of the *nob9* OPL increases from P6 to P10; however, it subsequently decreases rapidly. Hematoxylin and eosin staining of retinal sections in vitro (Fig. 3) were consistent with OCT outcomes in vivo (Fig. 4). These results indicate that the disease in these mice could be early-onset and that the photoreceptor synapse degeneration progresses rapidly.

The *nob2* mice display stable negative a-wave amplitudes at 3–15 months of age (Chang et al., 2006). The phenotype of the *nob9* mouse is more severe than that of the *nob2* strain. As shown in Fig. 5, scotopic ERG a-wave amplitudes of *nob9* eyes deteriorate with increasing age. The similarity between the C57BL/6J and *CngaS*$^{-/-}$ ERGs indicates that the scotopic a-wave is rod-dominant (Seeliger et al., 2001). Despite a reduction of rod function, the *nob9* retina displays almost normal ONL and outer segment thickness. Since rods account for more than 97% of murine photoreceptors (Cangiano et al., 2012), our morphological results indicate that *nob9 Cacna1f* mutations do not eradicate rods; their phenotype is not similar to the photoreceptor degeneration in common retinitis pigmentosa.

Compared to *nob2* mice (Chang et al., 2006), photopic ERGs in *nob9* mice are more impaired. Stained by cone-specific markers, *nob9* retinas showed decreased M-and S-opsin numbers with increasing age, while the progressive loss of M-opsins was more pronounced. Almost no M-opsins were detected at 14 months, the oldest age examined. In humans, blue cone monochromatism is caused by mutations in the genes that encode red and green opsins

on chromosome X (Kellner et al., 2004). We do not know whether *Cacna1f* mutations of the *nob9* mouse lead to abnormalities in X-chromosomal opsin genes. At the oldest time point, *nob9* retinas display some residual cones with S-opsins abnormally migrated to inner photoreceptor segments. Mislocalization of cone opsins was seen not only in *nob9* retinas but also in some photoreceptor deficiency models such as Cnga3-mutant *cpfl5* (Dai et al., 2017) and Rpe65-mutant *rd12* mice (Li et al., 2011). No UV ERG responses could be detected in *nob9* retinas indicating that the residual S-cones are also functionally abnormal. A study in zebrafish confirmed that *Cacna1f* is also vital for the functional assembly and maintenance of cone photoreceptors (Jia et al., 2014).

With respect to the *nob9* fundus, some small white dots are visible by the age of 8 months. Detailed investigations are required to delineate whether this retinal abnormality is due to the degeneration of photoreceptors or other tissues.

Congenital stationary night blindness (CSNB) is generally believed to represent a group of genetically heterogeneous retinal disorders (Miyake et al., 1986). X-linked CSNBs are classified into a complete (CSNB1) and an incomplete (CSNB2) form, based on genetic analyses and functional differences in ERGs. Mutations in *Cacna1f* cause the CSNB2 (Bech-Hansen et al., 1998). Transmission defects from photoreceptors to depolarizing bipolar cells can cause ERG b-wave abnormalities. Some CSNB2 patients with gradual photoreceptor degeneration may doubt the progressive nature of their vision impairment. One reason for this discrepancy could be the fact that the lifespan of humans is much longer than that of mice, therefore photoreceptor degeneration might have a later onset or might remain unnoticed for a long time. This study may provide useful clues for mutation screenings in CSNB2-like patients, especially those with unusually severe phenotypes and progressive photoreceptor impairment. Recently, the *Cacna1f* mRNA expression and its final protein product have been found in retina, as well as skeletal muscle, bone marrow, spinal cord, spleen, thymus (McRory et al., 2004), and lymphocytes (Omilusik et al., 2011). Clinically, Duchenne/Becker muscular dystrophy (Pillers et al., 1999) and benign adult familial myoclonic epilepsy (Manabe et al., 2002) can simultaneously exhibit a CSNB2-like negative ERG phenotype.

As a new model for *Cacna1f* mutation, the *nob9* mouse shows additional photoreceptor degeneration with increasing age. We have identified a new mutation in the L-type calcium channel subunit *Cacna1f* which is responsible for the observed morphological and functional changes. With the identification and characterization of the *nob9* mouse, a gene therapy project is underway to investigate if delivery of a wild-type *Cacna1f* gene can restore the retinal structure and function in this model.

Acknowledgments

We thank Dr Song Mao (Department of Ophthalmology, University of Florida, Gainesville, USA) for helpful assistance and advice on cryosectioning.

This work was supported by the Natural Science Foundation of Zhejiang Province of China [NO. LY15H120002]; National Natural Science Foundation of China [NO. 81371060]; and National Institutes of Health (NIH) grants [NO. EY023543, NO. EY019943]. The funders had no involvement throughout the study.

Abbreviations:

CSNB	congenital stationary night blindness
ERG	electroretinogram
INL	inner nuclear layer
IPL	inner plexiform layer
M-opsin	middle-wavelength opsin
NL	neuroblastic layer
nob	no b-wave
OCT	optical coherence tomography
ONL	outer nuclear layer
OPL	outer plexiform layer
PCR	polymerase chain reaction
PNA	peanut agglutinin
S-opsin	short-wavelength opsin
WT	wild-type

References

Bayley PR., Morgans CW, 2007 Rod bipolar cells and horizontal cells form displaced synaptic contacts with rods in the outer nuclear layer of the nob2 retina. J. Comp. Neurol 500, 286–298. [PubMed: 17111373]

Bech-Hansen NT, et al., 1998 Loss-of-function mutations in a calcium-channel alpha1-subunit gene in Xp11.23 cause incomplete X-linked congenital stationary night blindness. Nat. Genet 19, 264–267. [PubMed: 9662400]

Boycott KM, et al., 2001 A summary of 20 CACNA1F mutations identified in 36 families with incomplete X-linked congenital stationary night blindness, and characterization of splice variants. Hum. Genet 108, 91–97. [PubMed: 11281458]

Buffone GJ., Darlington GJ., 1985 Isolation of DNA from biological specimens without extraction with phenol. Clin. Chem 31, 164–165. [PubMed: 3965205]

Cangiano L, et al., 2012 The photovoltage of rods and cones in the dark-adapted mouse retina. J. Physiol 590, 3841–3855. [PubMed: 22641773]

Catterall WA, et al., 2008 Inherited neuronal ion channelopathies: new windows on complex neurological diseases. J. Neurosci 28, 11768–11777. [PubMed: 19005038]

Chang B, et al., 2006 The nob2 mouse, a null mutation in Cacna1f: anatomical and functional abnormalities in the outer retina and their consequences on ganglion cell visual responses. Vis. Neurosci 23, 11–24. [PubMed: 16597347]

Dai X, et al., 2016 Effects of Subretinal Gene Transfer at Different Time Points in a Mouse Model of Retinal Degeneration. PLoS One 11, e0156542. [PubMed: 27228218]

Dai X, et al., 2017 Long-term retinal cone rescue using a capsid mutant AAV8 vector in a mouse model of CNGA3-achromatopsia. PLoS One 12, e0188032. [PubMed: 29131863]

Doering CJ, et al., 2008 Modified Ca(v)1.4 expression in the Cacna1f(nob2) mouse due to alternative splicing of an ETn inserted in exon 2. PLoS One 3, e2538. [PubMed: 18596967]

Fisher SE, et al., 1997 Sequence-based exon prediction around the synaptophysin locus reveals a gene-rich area containing novel genes in human proximal Xp. Genomics 45, 340–347. [PubMed: 9344658]

Jacobs GH, Williams GA, 2007 Contributions of the mouse UV photopigment to the ERG and to vision. Doc. Ophthalmol 115, 137–144. [PubMed: 17479214]

Jia S, et al., 2014 Zebrafish Cacna1fa is required for cone photoreceptor function and synaptic ribbon formation. Hum. Mol. Genet 23, 2981–2994. [PubMed: 24419318]

Kellner U, et al., 2004 Blue cone monochromatism: clinical findings in patients with mutations in the red/green opsin gene cluster. Graefes Arch. Clin. Exp. Ophthalmol 242, 729–735. [PubMed: 15069569]

Knoflach D, et al., 2013 Cav1.4 IT mouse as model for vision impairment in human congenital stationary night blindness type 2. Channels (Austin) 7, 503–513. [PubMed: 24051672]

Knoflach D, et al., 2015 Gain-of-function nature of Cav1.4 L-type calcium channels alters firing properties of mouse retinal ganglion cells. Channels (Austin) 9, 298–306. [PubMed: 26274509]

Li X, et al., 2011 Gene therapy rescues cone structure and function in the 3-month-old rd12 mouse: a model for midcourse RPE65 leber congenital amaurosis. Invest. Ophthalmol. Vis. Sci 52, 7–15. [PubMed: 21169527]

Liu X, et al., 2013 Dysregulation of Ca(v)1.4 channels disrupts the maturation of photoreceptor synaptic ribbons in congenital stationary night blindness type 2. Channels (Austin) 7, 514–523. [PubMed: 24064553]

Lodha N, et al., 2010 Congenital stationary night blindness in mice - a tale of two Cacna1f mutants. Adv. Exp. Med. Biol 664, 549–558. [PubMed: 20238058]

Manabe Y, et al., 2002 Benign adult familial myoclonic epilepsy (BAFME) with night blindness. Seizure 11, 266–268. [PubMed: 12027575]

Mansergh F, et al., 2005 Mutation of the calcium channel gene Cacna1f disrupts calcium signaling, synaptic transmission and cellular organization in mouse retina. Hum. Mol. Genet 14, 3035–3046. [PubMed: 16155113]

Matthews G, Fuchs P, 2010 The diverse roles of ribbon synapses in sensory neurotransmission. Nat. Rev. Neurosci 11, 812–822. [PubMed: 21045860]

McRory JE, et al., 2004 The CACNA1F gene encodes an L-type calcium channel with unique biophysical properties and tissue distribution. J. Neurosci 24, 1707–1718. [PubMed: 14973233]

Michalakis S, et al., 2014 Mosaic synaptopathy and functional defects in Cav1.4 heterozygous mice and human carriers of CSNB2. Hum. Mol. Genet 23, 1538–1550. [PubMed: 24163243]

Miyake Y, et al., 1986 Congenital stationary night blindness with negative electroretinogram. A new classification. Arch. Ophthalmol 104, 1013–1020. [PubMed: 3488053]

Morgans CW, 2001 Localization of the alpha(1F) calcium channel subunit in the rat retina. Invest. Ophthalmol. Vis. Sci 42, 2414–2418. [PubMed: 11527958]

Morgans CW, et al., 2005 Photoreceptor calcium channels: insight from night blindness. Vis. Neurosci. 22, 561–568. [PubMed: 16332266]

Omilusik K, et al., 2011 The Ca(v)1.4 calcium channel is a critical regulator of T cell receptor signaling and naive T cell homeostasis. Immunity 35, 349–360. [PubMed: 21835646]

Pardue MT, Peachey NS, 2014 Mouse b-wave mutants. Doc. Ophthalmol 128, 77–89. [PubMed: 24395437]

Pillers DA, et al., 1999 Duchenne/Becker muscular dystrophy: correlation of phenotype by electroretinography with sites of dystrophin mutations. Hum. Genet 105, 2–9. [PubMed: 10480348]

Regus-Leidig H, et al., 2014 Photoreceptor degeneration in two mouse models for congenital stationary night blindness type 2. PLoS One 9, e86769. [PubMed: 24466230]

Seeliger MW, et al., 2001 New views on RPE65 deficiency: the rod system is the source of vision in a mouse model of Leber congenital amaurosis. Nat. Genet 29, 70–74. [PubMed: 11528395]

Sterling P, Matthews G, 2005 Structure and function of ribbon synapses. Trends Neurosci. 28, 20–29. [PubMed: 15626493]

Waldner DM, et al., 2018 Cone dystrophy and ectopic synaptogenesis in a Cacna1f loss of function model of congenital stationary night blindness (CSNB2A). Channels (Austin) 12, 17–33. [PubMed: 29179637]

Wang J, et al., 2015 Carposina sasakii (Lepidoptera: Carposinidae) in its Native Range Consists of Two Sympatric Cryptic Lineages as Revealed by Mitochondrial COI Gene Sequences. J. Insect Sci 15, pii:85. [PubMed: 26136498]

Highlights:

- Identification of a new *Cacna1f* mutation in a mouse strain
- The mutation leads to a frame-shift in exon 14
- The murine phenotype is similar to that in congenital stationary night blindness
- The mutation causes a degeneration of the outer plexiform layer
- Middle-wavelength opsins are nearly absent in this mouse model

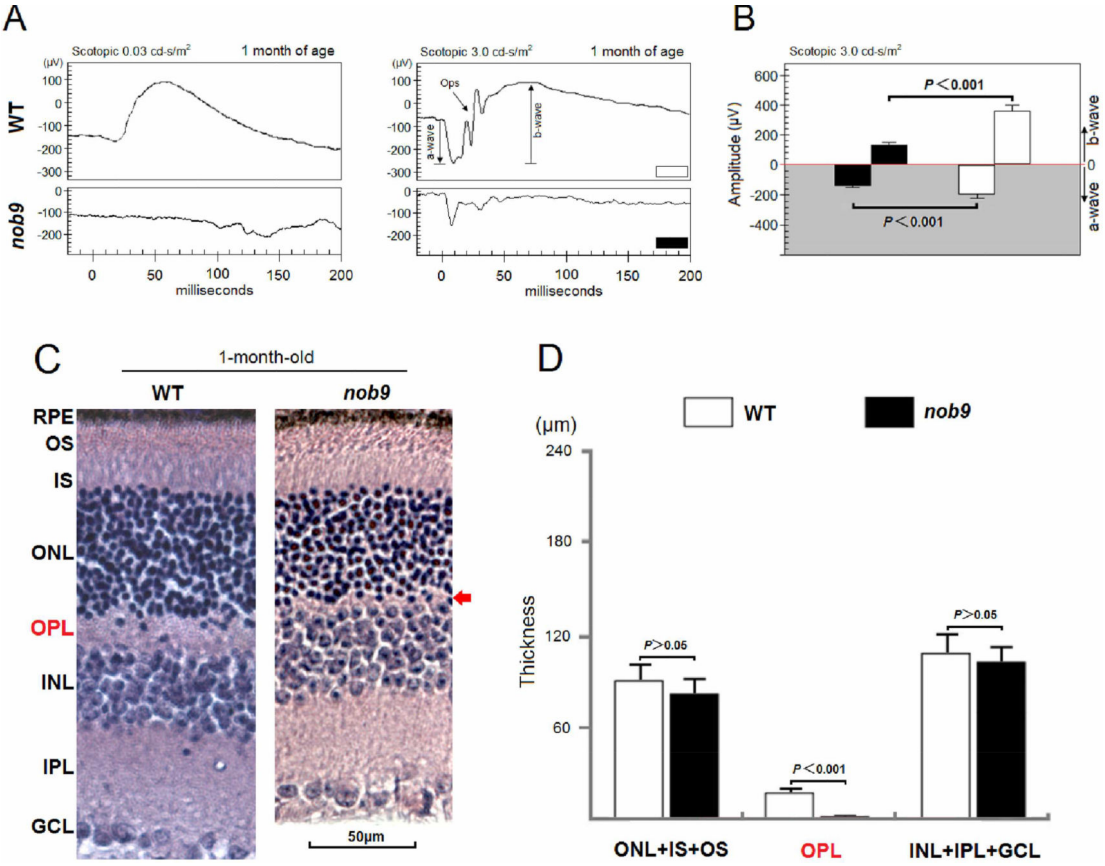

Fig. 1. Electroretinographic and morphological abnormalities in the 1-month-old *nob9* retina.

(A) Comparison of scotopic ERGs recorded from a *nob9* mouse and WT control. (B) The a- and b-wave amplitudes of scotopic 3.0 cd-s/m^2 ERG. (C) Representative histological sections of *nob9* and WT retinas. (D) Thickness measurements of various retinal layers. At 1 month, the *nob9* retina displays a reduced OPL thickness (arrow), but no apparent abnormalities were seen in other layers. RPE, retinal pigment epithelium; OS, outer segment; IS, inner segment; ONL, outer nuclear layer; OPL, outer plexiform layer; INL, inner nuclear layer; IPL, inner plexiform layer; GCL, ganglion cell layer; WT, wild-type C57BL/6J. *Columns* and *bars* represent mean ± SD (n = 6).

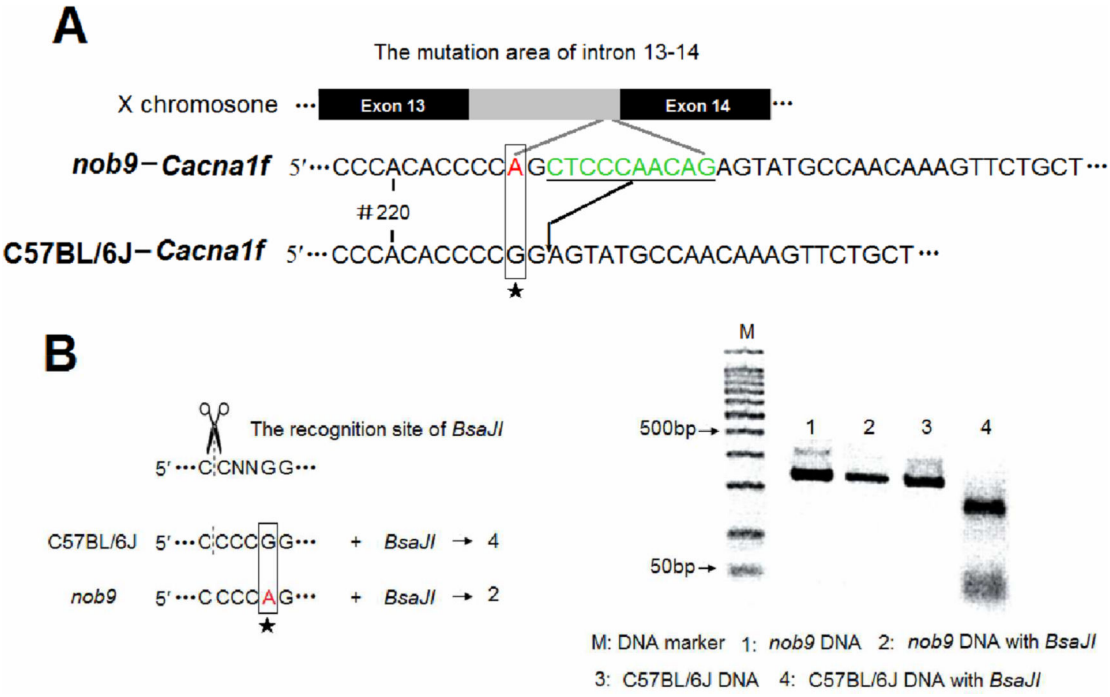

Fig. 2. Identification of *Cacna1f* mutations in the *nob9* mouse.

(A) Sequence analysis of *Cacna1f* DNA from the *nob9* mouse and WT control. The sequence variants for the *nob9* involved both a single nucleotide G to A transition (in red) and a 10-nucleotide insertion (in green) within intron 13–14. (B) PCR products produced by *BsaJI* digestion confirming the G mutation as shown in (A). As a restriction endonuclease, *BsaJI* is able to recognize and cleave DNA at “CCNNGG” sites.

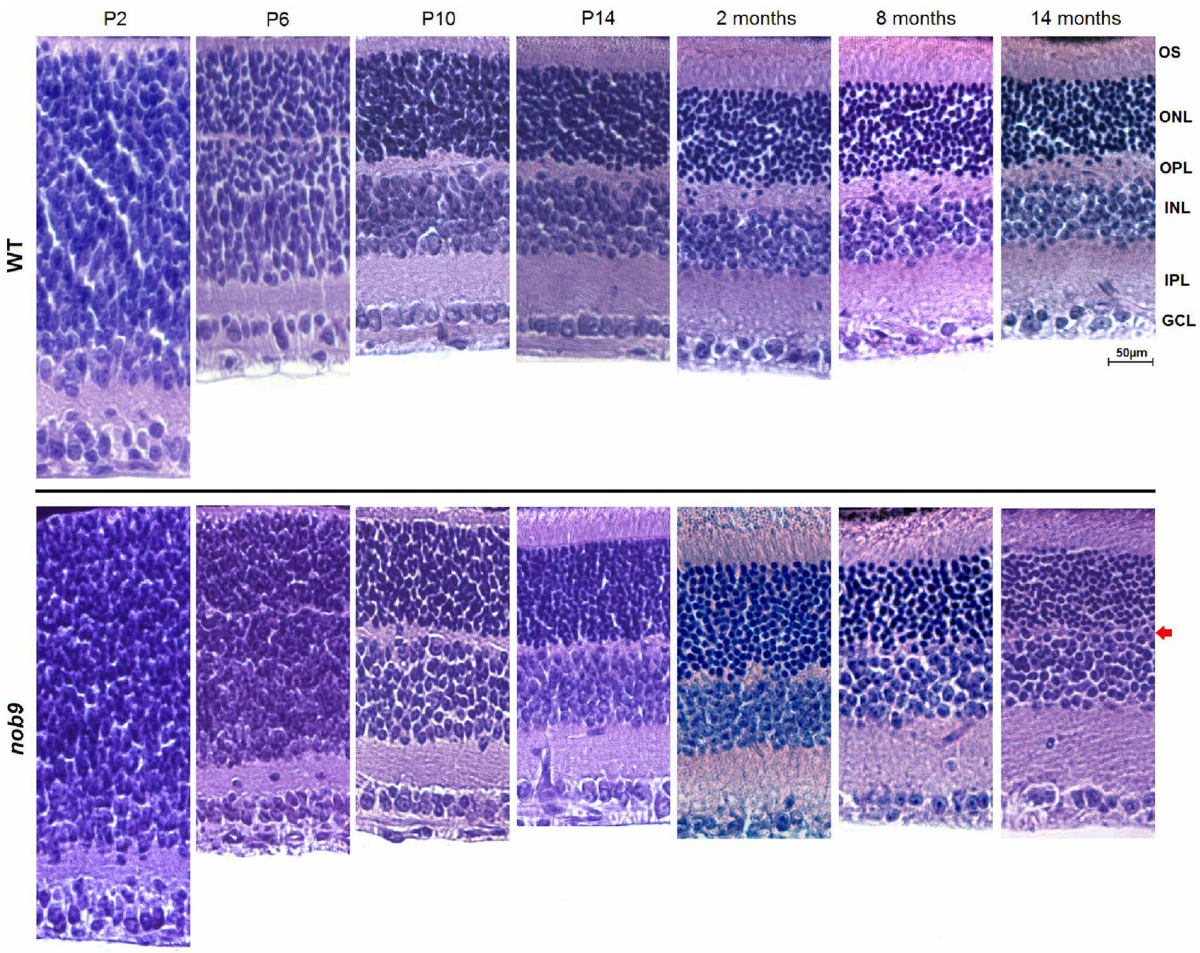

Fig. 3. Representative histological sections of WT and *nob9* retinas at age P2, P6, P10, P14, and 2, 8, and 14 months.

The thickness of the *nob9* OPL decreases at P14 and is almost absent by the age of 2 to 14 months (arrow). Age-matched WT mice were used as control. P, postnatal day.

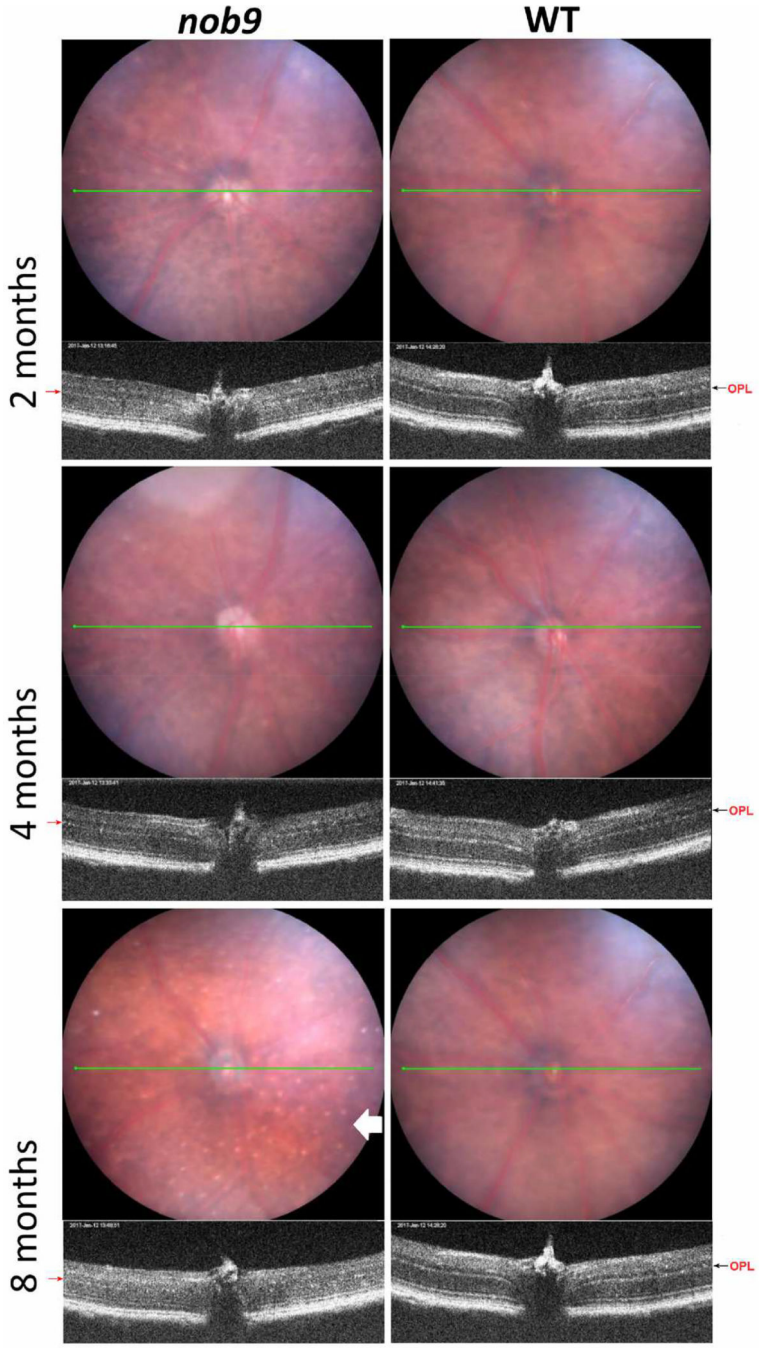

Fig. 4. Fundus and OCT images of WT and *nob9* eyes at the age of 2, 4, and 8 months.

OCT images show that *nob9* retinas display a reduction of OPL thickness already at 2 and 4 months, and the space between ONL and INL is almost undetectable by the age of 8 months (red arrow). The *nob9* (left column) eye had a normal fundus at 2 and 4 months. At 8 months, some small white dots were noted (white arrow).

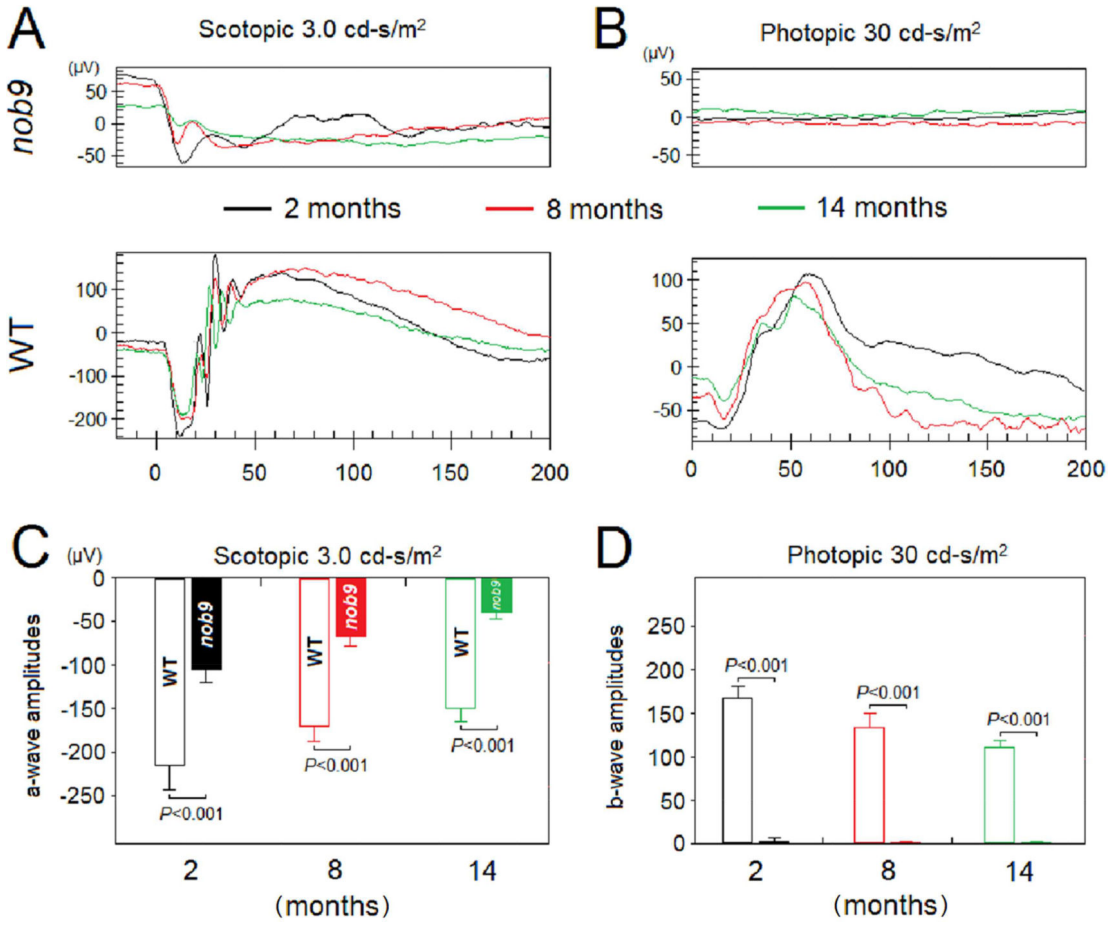

Fig. 5. Scotopic and photopic ERGs of WT and *nob9* eyes at 2, 8, and 14 months.

(A) Scotopic ERGs detected in the two strains. (B) Photopic ERGs recorded in *nob9* and WT mice. Scotopic a-wave (C) and photopic b-wave amplitudes (D) were measured. Age-matched WT eyes were used as controls. *Columns* and *bars* represent mean ± SD (n = 6).

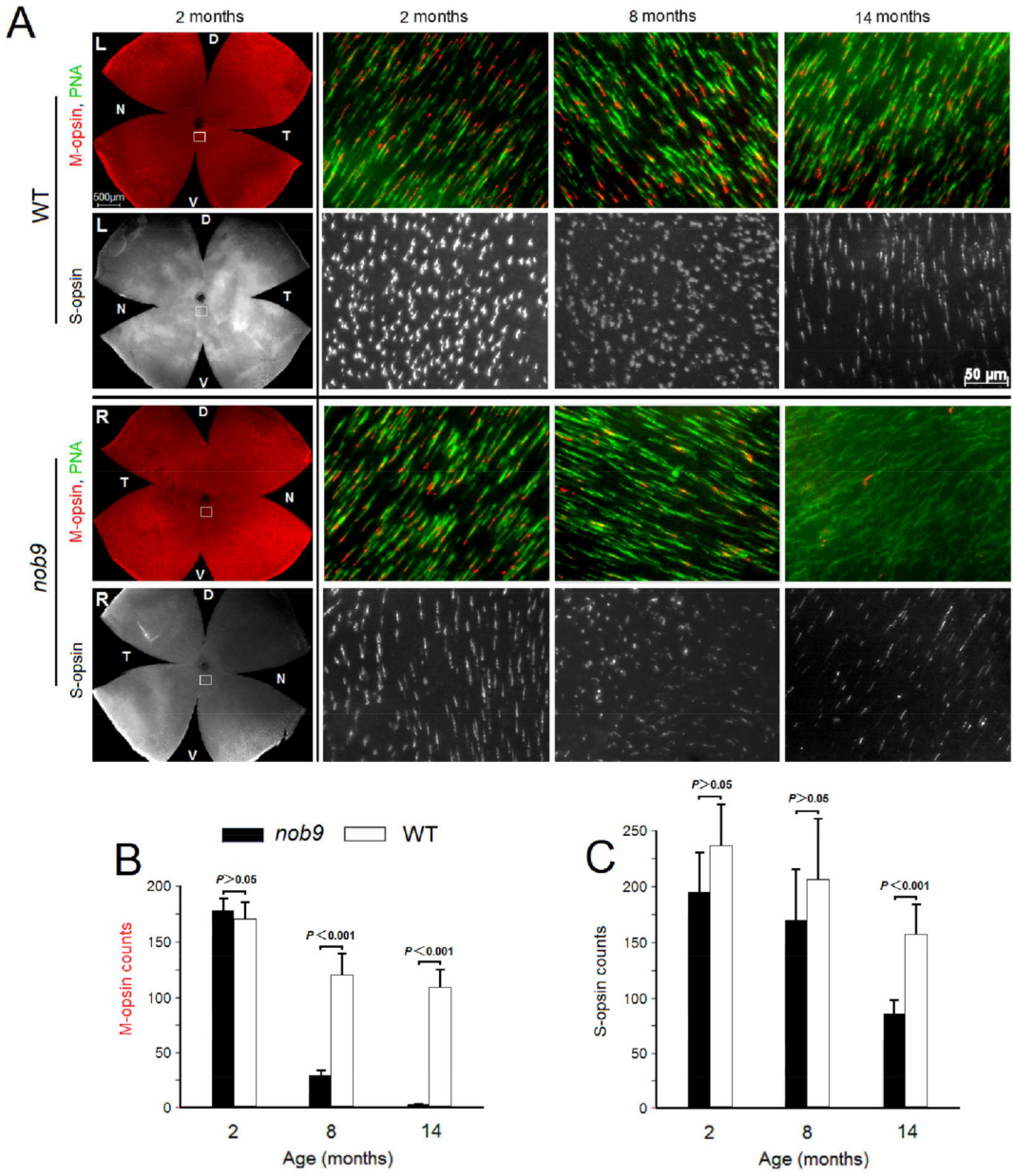

Fig. 6. Whole-mount immunohistochemistry of retinas from WT and *nob9* mice at 2, 8, and 14 months.

Retinal cone-specific PNA (green), M-opsins (red) and S-opsins (white) of the posterior pole segments were examined at a specific location (A), and the two types of cone opsins were counted (B, C). Age-matched WT eyes were used as controls. L, left eye; R, right eye; D, dorsal; V, ventral; T, temporal; N, nasal. *Columns* and *bars* represent mean ± SD (*n* = 6).

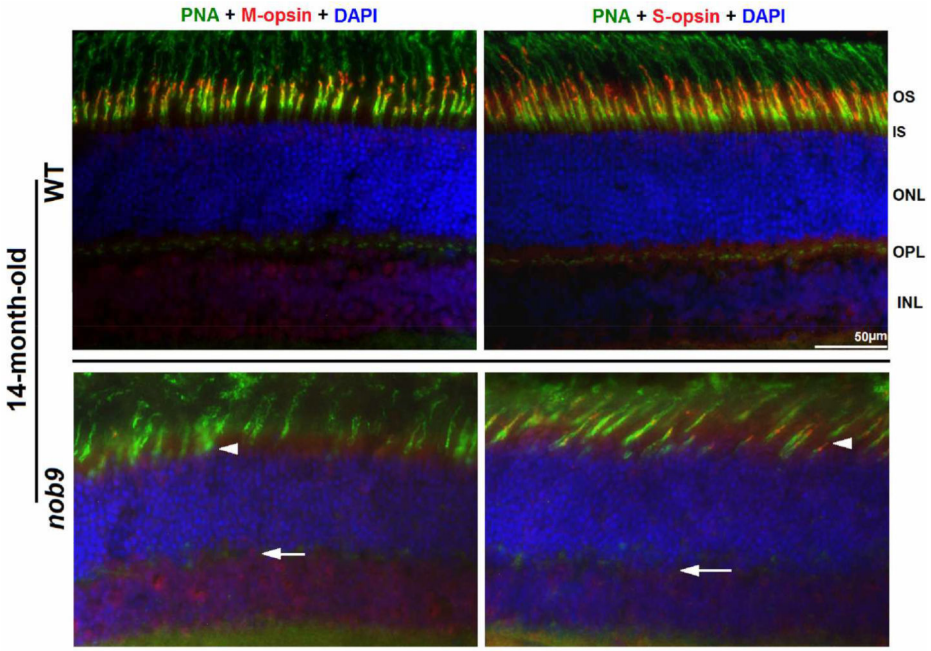

Fig. 7. Immunohistochemistry of retinas from WT and *nob9* mice at 14 months.

Retinal cone-specific PNA (green), M- or S-opsins (red) of the posterior pole segments were imaged at a defined location (about 0.3 mm ventral to the optic nerve). Between ONL and INL, the OPL is almost absent in the *nob9* retina (arrows). Almost no M-opsins are detected, and some PNA and S-opsins migrate to inner segments of photoreceptors (arrowheads). Age-matched WT eyes were used as controls.

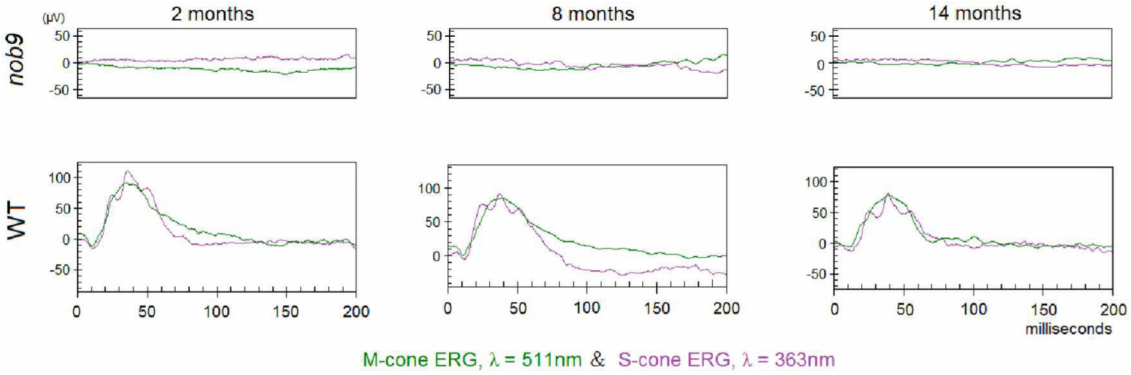

Fig. 8. M- and S-cone ERGs of WT and *nob9* eyes at 2, 8, and 14 months.

M-cone ERGs were elicited by green light with a strength of 0.75 cd-s/m^2, while S-cone ERGs were elicited by UV light with a strength of 3.00 mW-s/m^2.

Table 1

Primers used to screen the murine *Cacna1f* gene.

Primer No.	Forward (5′–3′)	Reverse (5′–3′)
CA-1	CCTTATATCTCCTGAGGAGG	AGATCCCAGGAAGTAGCATG
CA-2	TCAATTCCATCATGAAGGCG	GCGTGTACAGCTAGCCATGG
CA-3	CTCCCAGCCAGTGACACTGG	AGTTGCCACAGATGAAGAGG
CA-4	TCCTGACTGGGTGAGGATTGG	TGGATGCCGAAGGAGATGAG
CA-5	AGATGACAGTGTTTGGGGCC	GCTAGGGCCACCGTGTTGAG
CA-6	GCGCCAGTGTGTGGAATATG	GCTGATGAAGTAGACGATGG
CA-7	CAGGTGTGCCACTGGTGAGG	GCCAGCCTGTATCACACTGG
CA-8	AATCTCGATGGAACTCTAGG	GTAAGGATTTAGAGGGCATG